Phosphatic Carbonate Shale of the "Bird's Nest Saline Zone", Upper Green River Formation, Uinta Basin, Utah

10

Dave Keighley

Abstract

In aqueous depositional systems, phosphorus (P) is highly mobile and is readily reworked back into the water column after initial sedimentation. As a result, during deposition of most lacustrine sedimentary successions, gross P sedimentation typically is not much greater than gross P release, leading to low net P abundance. Such low abundances predominate in a 200 m-thick lacustrine succession of variably shaley, evaporitic, and organic-rich carbonate mudstone from the upper member of the Green River Formation in the Uinta Basin of Utah. However, the succession also includes thin but highly enriched phosphatic horizons that represent marked aberrations in the prevailing depositional and immediate subsurface diagenetic environment. This contribution details one carbonate shale bed, containing calcite pseudomorphs, that is equated with the nahcolite-bearing "bird's-nest saline zone" of the upper Green River Formation. X-ray diffraction analyses and scanning electron microscopy record the P-enrichment as interstitial microcrystalline aggregates of calcium fluorapatite. The calcium fluorapatite also partly replaces precursor grains, forms a grain coating around some silicate grains and occurs alongside abundant displacive and pseudomorphing crystals of calcite, and rhombic dolomite.

At high pH, which would have promoted nahcolite precipitation in the deeper part of the lake, the presence of dissolved Mg^{2+} would have kinetically inhibited calcium fluorapatite precipitation even if P was at saturation. But, during evaporitic pumping adjacent to a sabkha environment, and possibly mediated by methanogenic bacteria, the formation of ferroan dolomite, and smectite, Mg^{2+} was removed from porewaters allowing calcium fluorapatite to crystallize.

D. Keighley (✉)
Department of Earth Sciences, University of New Brunswick, Fredericton, NB E3B 5A3, Canada
e-mail: keig@unb.ca

M.E. Smith, A.R. Carroll (eds.), *Stratigraphy and Paleolimnology of the Green River Formation, Western USA*, Syntheses in Limnogeology 1, DOI 10.1007/978-94-017-9906-5_10

10.1 Introduction

Phosphorus (P) can be preserved in the sedimentary record as a component of detrital mineral phases, fossil bone and shell. It is also released from dead and decaying organic matter, rarely from soluble inorganic phases, ultimately to be incorporated into the sediment pile of productive lakes and oceans as diagenetic mineral phases. However, most sedimentary successions have low phosphate content because much of what initially accumulates in sediment is continuously recycled back into the water column. Although the recycling mechanisms may temporarily break down, allowing for accumulation of sedimentary phosphate, there are few recorded examples of phosphatic beds in ancient lake strata.

This paper focuses on one example of elevated P in the variably shaley, variably marly mudstone (for brevity: "carbonate shale") of the upper Green River Formation (upper GRF), of the Uinta Basin in Utah (Fig. 10.1a). The example in question is associated with the uppermost occurrences of laminae-disruptive, coarsely crystalline calcite pseudomorphs that mark the Bird's Nest Saline Zone (BNSZ) in Gate Canyon, ~152 m above the base of the Mahogany Oil Shale Zone (MOSZ; Fig. 10.1b, c). The P occurs as aggregates of microcrystalline calcium fluorapatite (CFA) that infill interstices and replace detrital grains. The origin of this CFA is best interpreted to be the result of early diagenetic successions precipitating from hypersaline fluids in the shallow substrate, conditions not previously explained in detail for producing ancient lacustrine phosphates.

10.2 Previous Work

There are few, but varied, reports and interpretations of ancient lacustrine strata enriched in phosphatic minerals such as anapaite, $Ca_2Fe(PO_4)_2.4H_2O$; bradleyite, $Na_3PO_4.MgCO_3$; britholite, $(Ce,Ca)_5SiO_4(PO_4)_3(OH,F)$; fairfieldite $Ca_2(Mn,Fe)(PO_4)_2.2H_2O$; hydroxylapatite, or "hydroxyapatite", $Ca_5(PO_4)_3OH$; mitridatite $Ca_6(H_2O)_6[Fe_9O_6(PO_4)_9].3H_2O$; vivianite, $Fe_3(PO_4)_2.8H_2O$; and carbonate fluorapatite (CFA), or "francolite", $Ca_{10\text{-}a\text{-}b\text{-}c}\ Na_a\ Mg_b\ (PO_4)_{6\text{-}x}\ (CO_3)_{x\text{-}y\text{-}z}\ (CO_3,F)_y\ (SO_4)_z\ F_2$, where $2c = x - y - a$ = vacancies in the Ca site. In the Pliocene Glenns Ferry Fm. of Idaho, francolite is described replacing ooid and oncoid cortices and as a fibrous isopachous cement. These phosphatic ooidal sandstones are considered to have formed beneath an oxic microzone present at the sediment surface at times of lake transgression over nearshore sediment (Swirydczuk et al. 1981). In the Carboniferous Albert Formation of New Brunswick, phosphate enrichment mostly occurs in dolomitic oil shale but also in concretionary sandstone and fish-scale-bearing grey shale (Mossman et al. 1987). Britholite and anapaite have been identified and related to breakdown of algal matter with released P involved in mineral replacement (e.g. of calcite). Mudstone of the Miocene Cerdanya Basin of Spain contains veins, sphaerulite beds and septarian-like nodules of anapaite and fairfieldite. Precipitation of phosphate was determined to have occurred in open lacustrine mud with Ca-poor, circumneutral pH porewater fluctuating between oxic and anoxic (de las Heras et al. 1989). Phosphorite nodules in the Precambrian Diabaig Fm. of W Scotland contain microcrystalline francolite replacing detrital grains and infilling pores of silt laminae that also contain algal filaments and other eukaryotes and prokaryotes (Rodd and Stewart 1992; Strother et al. 2011). The preferred interpretation was that the francolite replaced micritic calcite below the oxic boundary (Rodd and Stewart 1992). The Štínik Fm. (Permian) of the Southern Gemeric Unit, Slovakia, contains CFA intraclasts and matrix within fining-upward sandstone–mudstone cycles. Turbidites are thought to have reworked stratabound phosphate that originally formed by the iron redox pump mechanism (Vozárová and Rojkovič 2000). In clayey diatomites from the Miocene of Thessaly, Greece, various phosphates occur as leaf and fecal replacements, veins and irregular concretions. The interpretation is that deep-lake sediment with anoxic circumneutral pH porewaters originally precipitated vivianite that was mostly altered to anapaite and hydroxylapatite as pore-

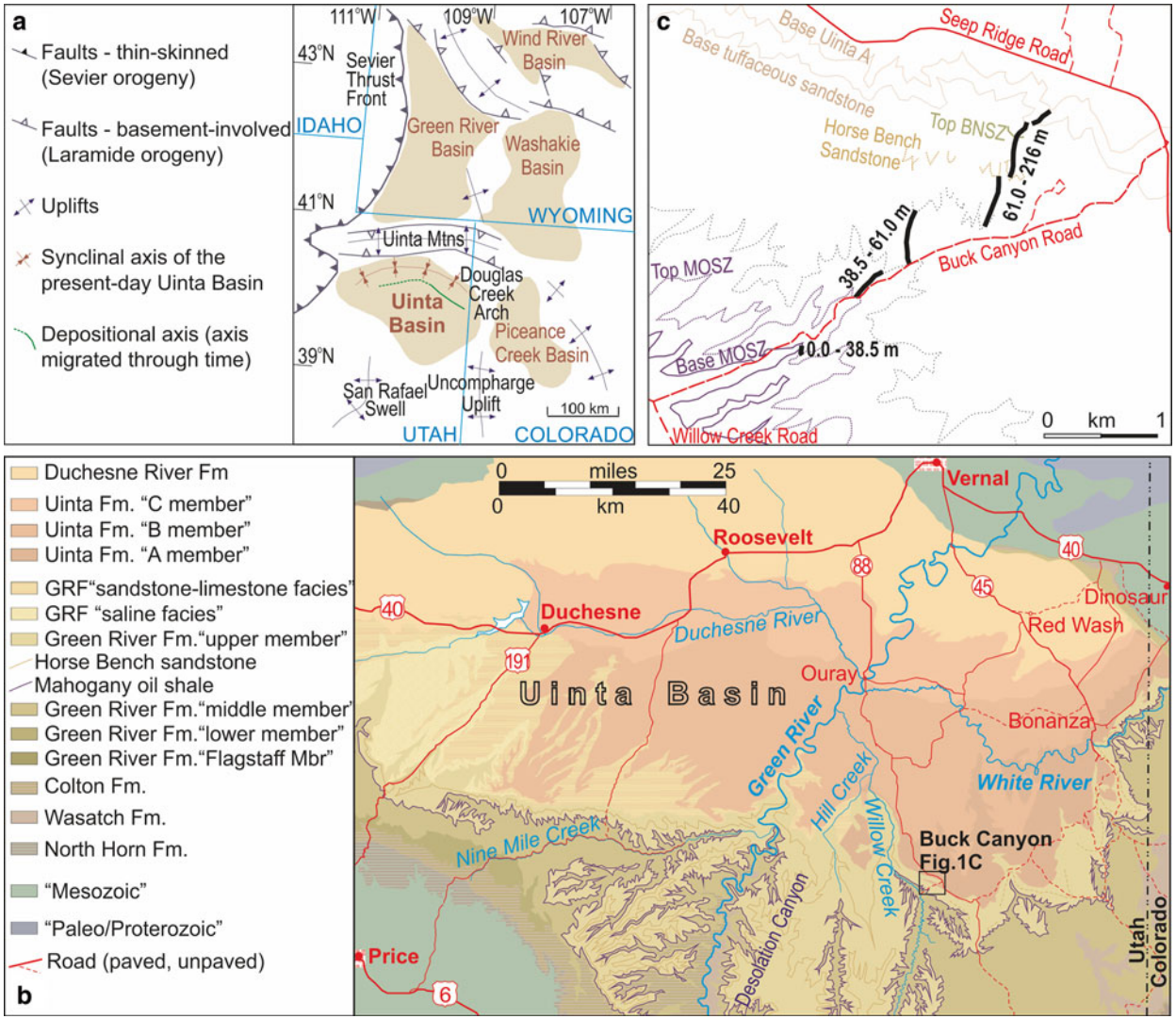

Fig. 10.1 (**a**) General location map of the major Laramide Basins in western United States (after Dickinson et al. 1988). Location of structural and depositional axes equate to Cashion (1995). (**b**) Geologic map for the Uinta Basin, adapted from Keighley (2013). (**c**) Location of the measured section at Buck Canyon

waters became more Ca-enriched; mitridatite was the result of recent weathering (Stamatakis and Koukouzas 2001). In all cases, anoxic decay of organic material in the substrate was thought to be a major contributor of dissolved P into porewaters. Abundant P has been identified in other lacustrine strata, but the host mineral and, or, its form or occurrence has not been detailed. For example, at Lake Manyara, Tanzania, Pleistocene bentonite clays interbed with phosphate. Fluorapatite was identified from XRD analyses but its diagenetic origin was not detailed (Mutakyahwa 2002). Phosphate minerals have also been reported in Eocene oil shale from Messel (Dietrich 1978); mid-Holocene sapropel from Lake Bosumtwi in West Africa (Talbot and Kelts 1986); Miocene marl of the Hula Basin, Jordan (Bein 1986); and Permian marl of the Ville Graben, France (Carasco 1989).

There have also been several studies from the Paleogene Laramide Basins of the western USA. The US Geological Survey's geochemical reference material, SGR-1, which is from part of the MOSZ of the adjacent Piceance Creek Basin, records an abundance of P at 0.328 ± 0.066 wt% (USGS website 2010; values always given as P_2O_5); the average in shale-rock composites is slightly less, ranging from 0.13 wt% (NASC, Gromet et al. 1984) to 0.16 wt% (PAAS, Taylor and McLennan 1985). In contrast, Tuttle (2009) encountered values of between 0.88 and 3.8 wt% P in seven of her ~150 sampled oil shale beds from above, below, and within the MOSZ, yet no other studies from this basin have encountered such anomalous values (Love 1964; Desborough et al. 1976; Saether et al. 1981). Phosphorus values of up to 18.2 wt% have been identified in interfingering sandstone, shale, and evaporite beds (that in core contain bradleyite) of the Wasatch Formation and GRF in the Greater Green River Basin of Wyoming (Fahey 1962; Love 1964; Mott and Drever 1983; Tuttle 2009). Bradley (in Fahey 1962, p. 62) suggested the "thin phosphate-rich zones in the Wilkins Peak Member may simply represent times when calcium carbonate precipitation was very rapid and swept out the phosphorus from the lake water, depositing it as tricalcium phosphate". Love (1964) proposed that the phosphates precipitated directly from periodically highly stratified hypersaline water columns.

In the Uinta Basin, most sampling has failed to encounter significant P-enriched horizons (Swanson 1960; Fabbi and Espos 1976; Tuttle 2009). Prior to Keighley (2013) and this paper, anomalously high values of P, at >8 wt% and >1 wt%, have been recorded only at stratigraphically unknown levels adjacent to Desolation Canyon, west of the Green River, and in a tributary of Hill Creek, ~12 km due west of the Buck Canyon study area (Love 1964); and as ~6 % apatite from XRD analysis of an oil shale close to Highway 191 (Bristow et al. 2012).

10.3 Geological Setting

10.3.1 Tectonic Setting of Paleogene Laramide Basins

The early Cenozoic Laramide Orogeny produced a series of extensive, primarily internally drained, nonmarine depositional basins in the western USA (Dickinson et al. 1988; Fig. 10.1a). N–S trending domal uplift of Mesozoic strata produced the saddle-like Douglas Creek Arch that formed a spill point between the Piceance Creek Basin and the Uinta Basin. Major uplift of E–W trending, thrust-fault-bounded basement rocks formed the Uinta Mountains (Bradley 1995) that separated these basins from the Greater Green River Basin to the north. The major erosional remnant of the Uinta Basin now forms a gentle asymmetrical syncline located in eastern Utah and westernmost Colorado; the fold axis, which also approximates with the depositional axis, is preserved toward the northern margin of the basin (Fig. 10.1a, b) in what, during the orogeny, was equivalent to a foreland-basin type setting.

10.3.2 Stratigraphy and Depositional Setting of the Uinta Basin

A typical lacustrine, tripartite vertical succession (Lambiase 1990) occurs in the Paleocene–Eocene of the Uinta Basin (Fig. 10.2). At the base, a predominantly coarse-clastic succession (Colton

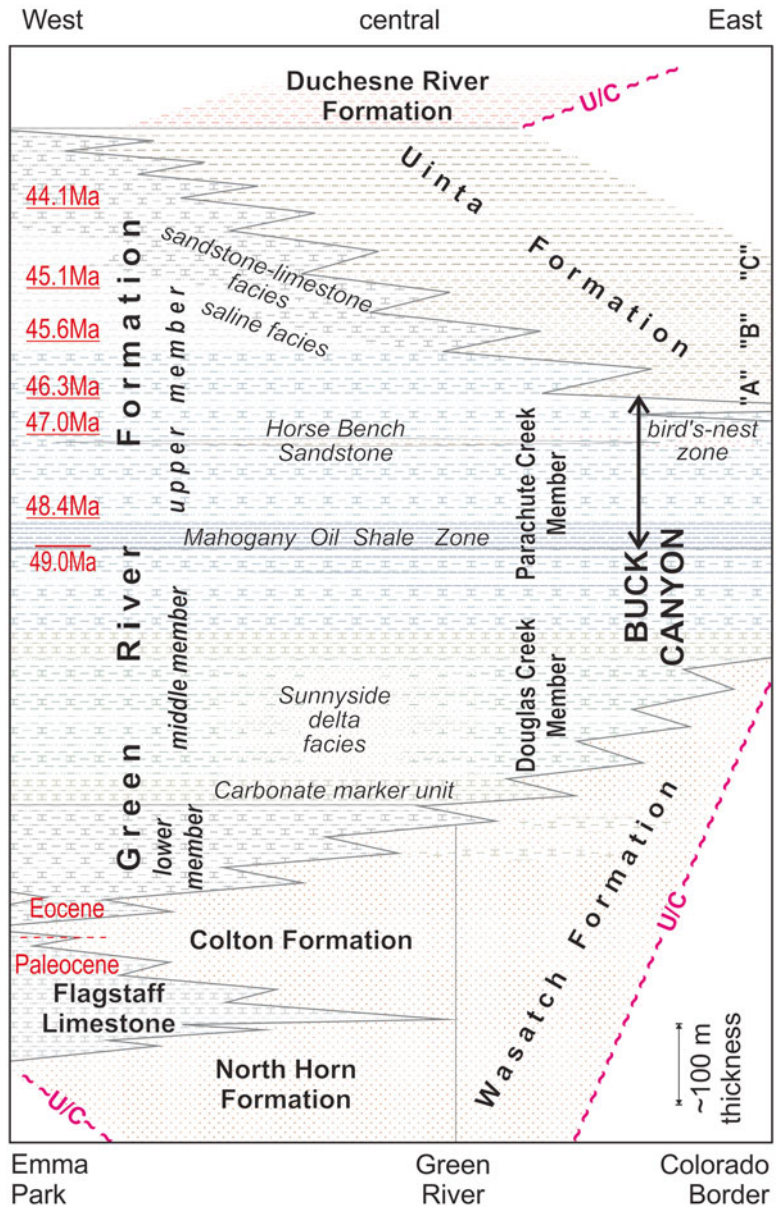

Fig. 10.2 Paleogene lithostratigraphic terminology for the lacustrine phases of the Uinta Basin (Adapted from Keighley 2013)

and Wasatch formations) is interpreted to be the initial alluvial inputs into the developing basin (Morris and Richmond 1992). Progressively upsection, variably shaley, variably carbonate-, evaporite-, and organic-rich mudstone, assigned to the GRF, cyclically onlaps toward the basin margin as the basin continued to deepen and the lake fluctuated, but generally expanded, in size (Keighley et al. 2003a). Oil shale is present at various stratigraphic levels with the richest oil shale beds concentrated within the approximately 30 m-thick MOSZ (Cashion 1967). The MOSZ is considered to mark the base of the informal upper member of the GRF (Morgan et al. 2002) and is traceable across most of the Uinta Basin. It is also correlated eastward into the Piceance Creek

Basin of Colorado. The MOSZ is interpreted to represent deepwater deposition during or immediately following the most prolonged period of merged lakes that periodically filled both depressions (as "Lake Uinta"), during and following the Early Eocene Climatic Optimum (Cashion 1967; Keighley et al. 2003b; Keighley and Flint 2008; Smith et al. 2008; Birgenheier and Vanden Berg 2011).

There are a few tuff beds present in the upper GRF. Sourced from numerous volcanic centers active in the western US at the time, they have been radiometrically dated and correlated across several kilometers of outcrop (Fig. 10.2; Smith et al. 2008). There is also one mappable sandstone interval, the Horse Bench Sandstone (HBS), which is most prominent west of the Green River and ~150 m above the MOSZ (Dane 1954; Dyni 1976; Remy 1992). In Willow Creek, the HBS lies ~120 m above the MOSZ but increasingly difficult to trace eastward. Eastward and northeastward across the basin, there is also a reduction in the variety and abundance of clay minerals in the upper GRF, along with less calcite, more dolomite and evaporite minerals (Dyni 1976). Near the White River southeast of Bonanza (Fig. 10.1), an interval with many (in outcrop, leached or altered to calcite) bedded nahcolite ($NaHCO_3$) nodules in a dolomitic shale matrix (Milton and Eugster 1959) was first described as the BNSZ by Cashion (1967). Birgenheier and Vanden Berg (2011) and Vanden Berg et al (2013) recently have also identified fracture-filling shortite ($Na_2Ca_2(CO_3)$), and described the BNSZ in core from north of Willow Creek. These authors note that near the basin depocenter the BNSZ is >110-m thick with nodules concentrated in two ~20-m thick intervals (termed the lower and upper saline zone) that are separated by an intervening succession rich in oil shale (termed the middle R-8 zone). Keighley (2013) correlates the interval to outcrop in Buck Canyon (Fig. 10.1c). The authigenic minerals identified in the BNSZ, and other saline units noted below, point to a lake that was evolving, cyclically, from a brackish into a hypersaline system, with evaporative phases containing warm (20–35 °C), sodic-carbonate dominated, low sulfate, high alkalinity waters (Bradley 1929; Milton and Eugster 1959; Tuttle and Goldhaber 1993; Dyni 1996; Smith et al. 2008; Vanden Berg et al. 2013).

Interbedded sandstone and mudstone of the Uinta Formation progressively caps the upper GRF, the contact being stratigraphically higher in the west than the east (Cashion 1967). This is due to pinch-outs of medium- to fine-grained sandstone (characteristic of the informal "A" member), which represent fluvial-deltaic deposits that gradually infilled both the Piceance Creek Basin and then the Uinta Basin from the northeast (Johnson 1981; Donnell 2009). To the west and upsection, finer grained sandstone and variegated mudstone (Uinta Fm., member "B") interfingers with a succession of mudstone, limestone, and yet more evaporite beds known as the "Saline Facies" and "Sandstone and Limestone Facies". Although included as part of the Uinta Fm. by Dane (1954) these facies intervals, along with thin tongues of Uinta Fm.-type sandstone, have been included by subsequent workers as part of the upper GRF (Fig. 10.2).

10.4 Methods

Detailed methodology is outlined in Keighley (2013). Briefly, at Buck Canyon (Fig. 10.1c), the exposed section has been logged at the bed (cm) scale (Fig. 10.3) with beds ascribed to one of four broad, end-member lithofacies, with more detailed lithofacies components identified where outcrop was of sufficient quality and extent (Table 10.1). For the original purpose of a chemostratigraphic study, samples were collected throughout the upper GRF, from the base of the MOSZ, through the BNSZ (including the calcite-pseudomorph bed, 152 m above MOSZ), and up into the basal Uinta A sandstone at the top of Seep Ridge (vertical thickness ~216 m). Sampling was systematic (every 4 m where there was outcrop, n = 52) with additional material collected at beds of particular interest (n = 37; total = 89 samples).

The elemental composition of all these samples was analyzed by Activation Laboratories,

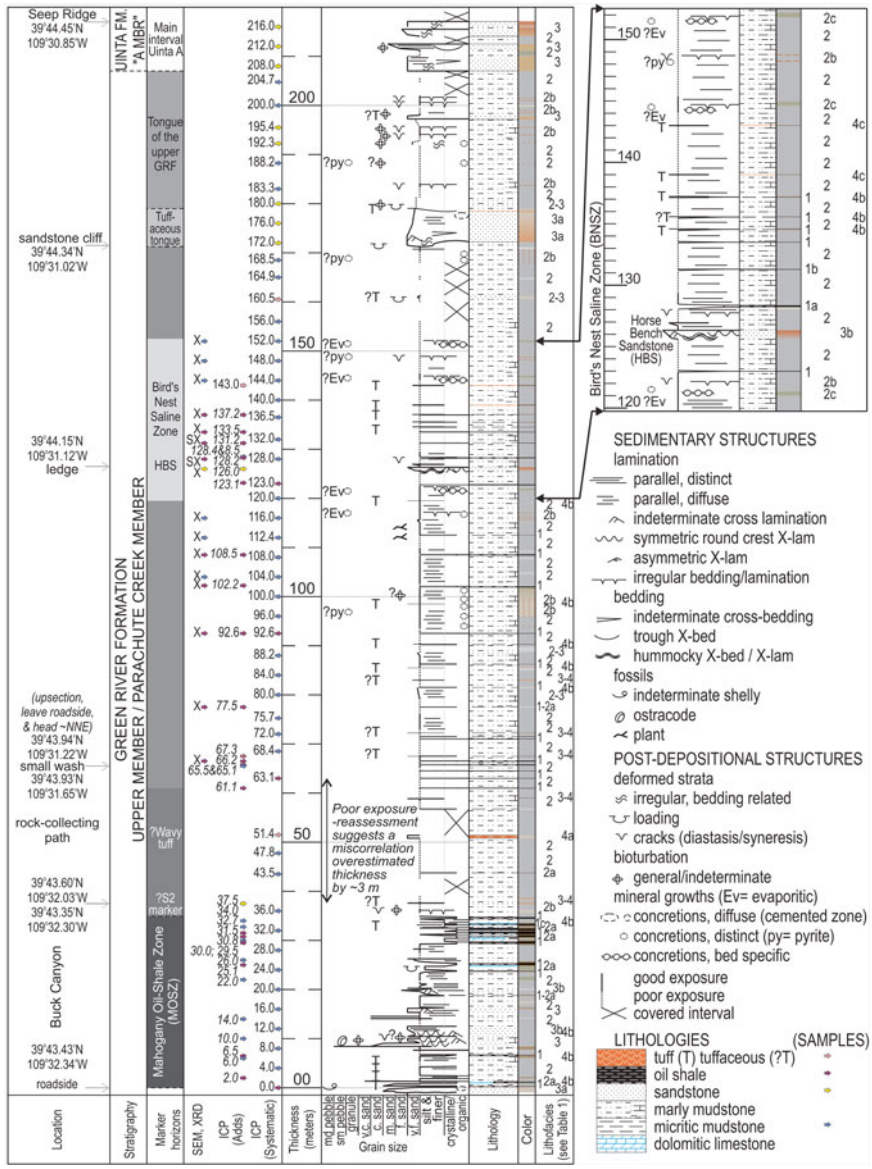

Fig. 10.3 Summary sedimentary log for the upper member of the Green River Formation, from the base of the Mahogany Oil Shale Zone up into the base of the Uinta Formation, adjacent to Buck Canyon (Adapted from Keighley 2013). See Table 10.1 for lithofacies codes

Canada, using a Varian Vista ICP-OES, calibrated using 7 prepared USGS and CANMET certified reference materials, and a Perkin Elmer SCIEX ELAN ICP/MS, all to a standard defined by ISO 17025. Selected samples were also analyzed by a Bruker AXS D8 solid state powder diffraction X-Ray Diffraction (XRD) system (at the University of New Brunswick) to determine major mineral phases present in the rock. Phase identification was made with a combination of windows-based software Bruker Eva and MDI Jade. Remaining sample chips from samples of greatest interest were split in half. One half was further cut and polished as a standard thin section along a cross-sectional surface. The other half was cut, polished and carbon coated along

Table 10.1 Lithofacies classifications for Buck Canyon (Adapted from Keighley 2013)

Lithofacies	Description	Interpretation	Occurrence
1. Oil shale	Typically 10–150 mm thick, purplish-black, to brown to dark gray, whitish weathering, micro- laminated to massive, commonly within one bed. Some paper shale. Interbedded and gradational with lithofacies 2, rarely with 4.	Settling of organic-rich detritus with minor (cyclic) clastic/evaporite input under eutrophic, no flow lacustrine conditions.	Most common in MOSZ (0–37.5 m) but sporadic up to 137.5 m.
	Component lithofacies identified where better exposed:		
	1a: Light-gray weathering, slightly domal caps (?stromatolitic).	1a: relatively shallow (photic) lake	1a not identified in the BNSZ
	1b: Angular crystals, ~2 mm diameter of (?pseudomorphing) carbonate	1b: evaporative, deep or (shallow) lake	
	1c: Internal micro-slumping ± microfaults	1c: remobilized, slumped, deep lake.	
2. Mudstone	Variably shaley, marly or variably calcareous/dolomitic, micro-laminated to apparently massive, can be variably colored (e.g., brown, olive, greenish gray, mid to light gray, and buff). Commonly soft-sediment deformed. Interbedded and gradational with all other lithofacies.	Cyclic suspended and washload deposition during low/no flow conditions with varied evaporite precipitation when minimal/no clastic input. Lacustrine low energy (offshore and low energy nearshore).	Common throughout. Predominant below 170 m.
	Component lithofacies identified where (rarely) better exposed:		
	2a: mostly massive, brown, dolomitic (micritic), whitish weathering	2a: clastic-starved lake	
	2b: rusted ?pyrite nodules ± cracks (diastasis) disrupting lamination, often in siltier strata, orange weathering	2b: anoxic shallow-water	
	2c: mm- to cm-scale calcite crystals (pseudomorphs) disrupting lamination in olive/ greenish grey shaley marlstone (evaporitic shale)	2c: evaporative conditions, likely shallow-water.	2c restricted to rare beds from 120 to 152.5 m

(continued)

Table 10.1 (continued)

Lithofacies	Description	Interpretation	Occurrence
3. Sandstone	Beds generally thin, very fine grained, buff, brown, orange or yellowish gray in color and variably calcareous. Diffuse low-angle cross beds and cross-laminations. Interbedded and gradational with lithofacies 2 and 4.	Suspended/saltating load deposition under waning aqueous flow.	Common above 200 m (Uinta A).
	Component lithofacies identified where better exposed:		
	3a: Lateral and vertical stacked lenticular beds occurs in fine-medium grained sandstone of the Uinta A. Asymmetric ripple cross-lamination, low-angle and planar cross bedding, and soft-sediment deformation structures.	3a: fluvial – sheetflood, possibly deltaic	3a occurs below the MOSZ and in the Uinta A.
	3b: Laterally extensive, tabular sandbodies of silty, highly calcareous, very-fine grained sandstone that quite sharply coarsen up from marly mudstone. Parallel lamination, wavy and hummocky cross-lamination.	3b: prograding lacustrine shoreface (offshore transition to nearshore)	3b Uncommon (but includes HBS at 126 m)
4. Tuff	Mostly massive, 10–450 mm thick, weather to a variably yellow to rusty-orange surface color, interbedded with lithofacies 2 or 3, and rarely capping or grading from lithofacies 1.	Volcanic ash falls	Sporadic throughout.
	Component lithofacies identified where better exposed:		
	Coarser-grained tuffs can be a dark gray color whereas others have		
	4a: light yellowish gray, dolomitic groundmass with occasional weathered (rusty) phenocrysts and irregular/wavy lamination	4a: Reworking/slumping/loading in shallow lacustrine conditions	4a not found in the BNSZ.
	4b: dark grey, fine to coarsely crystalline	4b, 4c: sub-aqueous settling in low-flow lacustrine conditions	
	4c: as for b, distinctly jointed "piano-key" structure.		

the counterface cross-section and on a bedding surface and analyzed with a Hitachi SU 70 FEG-SEM (resolution: 1.0 nm at 15 kV) with attached Oxford Instruments INCA solid-state EDS (also at UNB). The sample from 152 m required additional heating to 100 °C to eliminate problems in the vacuum chamber caused by degassing. Initial mapping of contiguous/adjoining ~300 µm by ~400 µm areas from top to bottom of each cross-sectional sample used the INCA mapping tool with 5 min acquisition times (~2 million counts), complemented with a BSE image of the same area. Selected INCA elemental maps were color coded and, using Corel software, overlain on the BSE image before being cropped, and montaged to help identify mineral phases. Areas or mineral associations of greater interest were mapped at greater resolution or spot analyzed. Spot size and interaction volume are dependent on the atomic number of the material being examined and the energy of the incident electron beam.

10.5 Buck Canyon Measured Section

10.5.1 General Description

A detailed description of the entire upper GRF in Buck Canyon is provided in Keighley (2013). In summary, and illustrated in Fig. 10.3, the MOSZ is ~35 m thick and comprises carbonate shale (lithofacies 2) irregularly interbedded with several <20 cm-thick beds of the other lithofacies (Table 10.1). Oil shale beds (lithofacies 1) are thickest and most common near the top of the MOSZ. The overlying 20–25 m is very poorly exposed on very gentle slopes, but is dominated by marly mudstone with only isolated ledges of tuffaceous sandstone and oil shale. A series of 5–20 cm-thick oil shale beds, typically spaced 0.5–2 m apart, mark the start of the better exposed section (starting ~60 m above base MOSZ). Thin beds of lithofacies 1 and 4 continue to outcrop at irregular intervals upsection, but lithofacies 2 still predominates. Keighley (2013) identifies the BNSZ, described in more detail below, between ~120 and ~152 m above base MOSZ. Upsection, lithofacies 2 continues to dominate, with rare lithofacies 4, until a 3–8 m thick, convolutely laminated, tuffaceous sandstone (lithofacies 3), with a deformed basal contact, is encountered ~171 m above base MOSZ. Overlying this sandstone is another interval dominated by lithofacies 2. The section is capped at the top of Buck Canyon by two stacked sandbodies (~207–216 m above base MOSZ) considered to form the basal beds of the main body of the Uinta Fm. "A member".

10.5.2 Description of the BNSZ

The base of the BNSZ is taken ~120 m above base MOSZ at an ~1 m-thick succession of olive-green weathering, laminated, carbonate shale that is variably disrupted by mm-scale, angular, displacive and pseudomorphed crystal aggregates now comprising calcite and rare dolomite: "mealstone" of Dyni (1996) (=lithofacies 2c). Two similar ~1 m-thick beds with calcite pseudomorphs occur at 144 and 152 m above base MOSZ. The top of the latter bed marks the top of the BNSZ at this locality. Most of the intervening BNSZ comprises variably exposed, gray, laminated carbonate shale (lithofacies 2). Sporadically, the carbonate shale contains intervals where laminae exhibit numerous lenticular, non-polygonal cracks filled with similar muddy sediment. Commonly in association with these cracks are variably spherical nodules, <1 cm diameter, that are highly rusted from surface weathering; rarely the nodule's core is pyritic (e.g., 148 m = lithofacies 2b). Variably brown, micritic, and diffusely laminated dolomitic mudstone (lithofacies 2a) is also present and locally grades into variably thin beds of oil shale (lithofacies 1) at several horizons, representing the middle R-8 zone. The uppermost 3 oil shale beds at 134.7, 135.7 and 137.2 m above base MOSZ are <5 cm-thick and are associated with similarly thin, gray, tuffaceous beds (lithofacies 4b). At 126 m above base MOSZ is the HBS, represented by a ~0.7 m-thick ledge of orange weathering, light gray, symmetrically rippled, coarsening-upward silty to very-fine-grained, and slightly tuffaceous calcareous sandstone (Fig. 10.4).

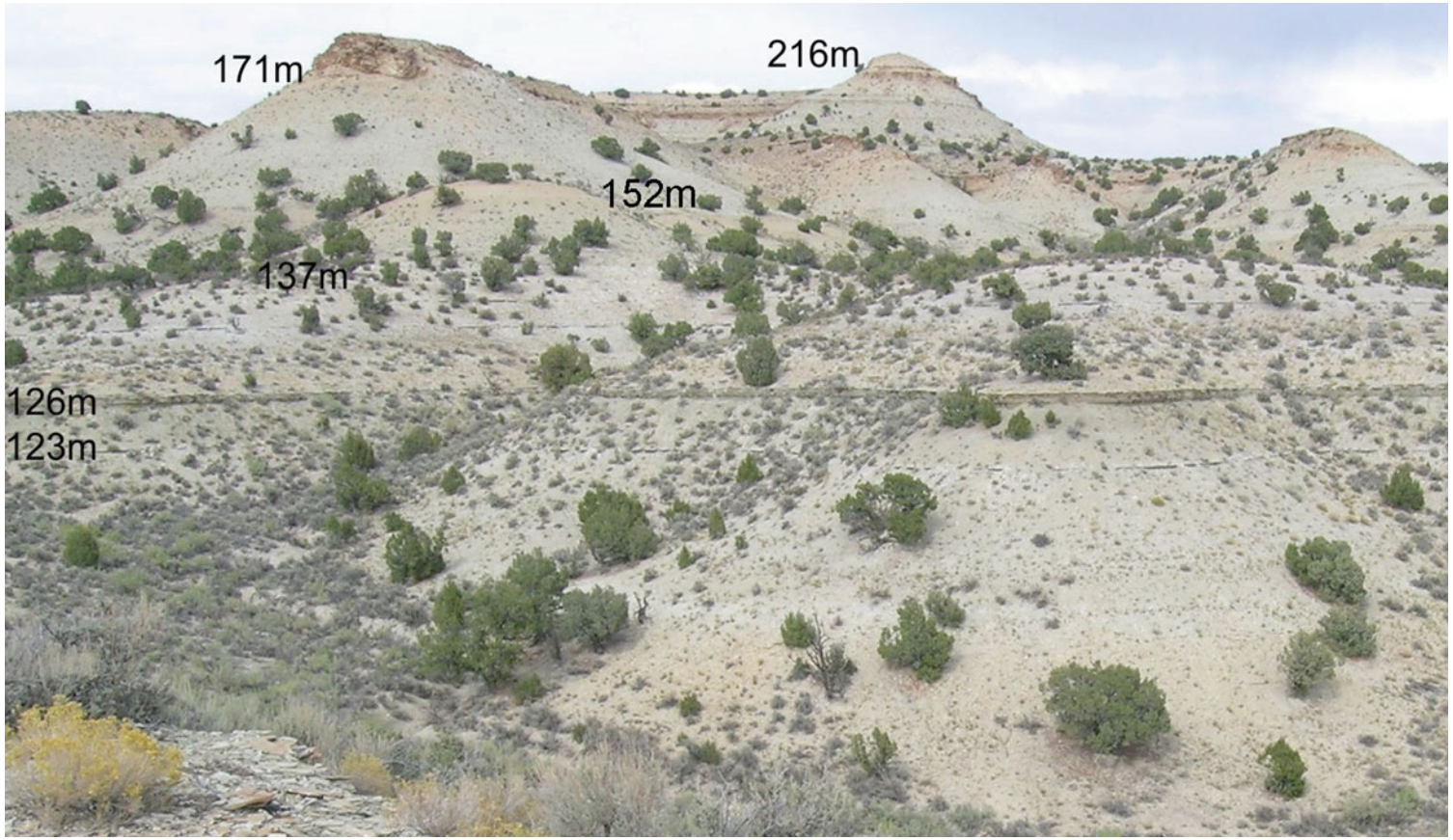

Fig. 10.4 The *upper* part of the measured section, including the bird's nest saline zone (BNSZ), is exposed west of Seep Ridge on the north side of Buck Canyon. The major ledge at 126 m is considered an eastern extension of the Horse Bench Sandstone. The tuffaceous sandstone at 171 m is highly deformed and locally can be loaded down into underlying carbonate shale by over 5 m

10.6 Sample Analyses

For the entire ICP dataset in Buck Canyon (n = 89), median P abundance is 0.08 wt%, whereas the mean is 0.72 wt% due to numerous anomalies. One such anomaly is the calcite-pseudomorph bed at 152 m that contains P at 5.57 wt%. Other anomalies, to be discussed in another paper, reach up to 9.47 wt% P, are distributed unevenly through the section, and represent samples from some of the oil shale beds (Fig. 10.5). For the entire dataset, the element additionally shows a high correlation co-efficient with uranium ($r = +0.78$, significant at $\alpha = 0.01$). Also of note, the Ca content is relatively constant throughout the section, but Mg values display an overall decline upsection (Fig. 10.5).

It should be noted that it is unlikely the above data will be inclusive of all phosphatic beds in the section: some beds may have been overlooked in the systematic sampling program (several were caught only in the additional sampling program, Fig. 10.5) and, since the phosphatization appears highly localized, the P abundance may have been diluted in some cases by inclusion in the sample of non-phosphatic horizons within a particular bed.

Nine samples from the BNSZ were further investigated by whole-rock XRD analysis. Table 10.2 shows that the fine-grained deposits of the BNSZ comprise a predominance of carbonate phases, with the silicon-bearing minerals collectively subordinate, and clay minerals (included in the sheet-silicates column of Table 10.2) generally negligible, i.e., compositionally the strata are mostly carbonate mudstone. The presence of CFA as the main P mineral is confirmed for the 152 m sample (Table 10.2; note that the calculated CFA percentage reflects the abundance exclusive of the organic phase). Zeolite occurs only in the 152 m sample, as the mineral faujasite. No pyrite was evident in this sample.

In hand specimen, angular crystals extensively and irregularly disrupt the mm-scale lamination. From thin-section optical petrography, these crystals are confirmed to be calcite, but their occasional orthorhombic-pyramidal cross-section indicates that at least some of the calcite is a pseudomorphic phase (Fig. 10.6). Most likely, the calcite is a replacement of shortite since this mineral has the appropriate precursor crystal form (orthorhombic hemimorphic, see fig 12 in Fahey 1962).

In SEM, typically sub-angular to sub-rounded grains of ~20–60 μm size (rarely exceeding 100 μm) map as combinations of Na, K, Al, and, or, Si (Fig. 10.7) and are considered to represent the silicate phases identified in XRD. Oriented elongate silicate grains and medium to coarse silt-sized silicate grains interlayer, at the ~0.25 mm scale, with larger (~100 μm) interlocking crystals to define the lamination. The latter include subpoikilotopic, subhedral crystals that map as Ca, O, and C (calcite), and euhedral-subhedral rhombic crystals containing Ca, Mg, with occasional minor Fe (high-Mg calcite or dolomite). No sodic (bi-) carbonates, siderite, pyrite or kerogenous stringers were identified by EDS, but very rare grains map as pure carbon (interpreted as coalified plant matter).

The matrix is generally an indistinguishable mix of crystals of Ca, P, F, Si, Al, Mg, minor Na, K, Fe, Ti, and rare traces of rare earth elements. Admixed sub-micron oblate hexagonal crystals may be a smectite or zeolite. The main CFA components, Ca, P and F, concentrate as rare detrital grains (Figs. 10.7 and 10.8a), along stringers (Fig. 10.8b), grain rims on selected silicate (mostly quartz) particles (Fig. 10.8c, d), and variably concentrated in scattered grain-shaped masses that might indicate variably altered precursor grains, possibly multi-mineralic (Fig. 10.8e, f).

Poikilotopic calcite encloses and post-dates the aforementioned phosphatized multi-mineralic grains (Fig 10.8f) and zoned, pitted rhombic dolomite (Fig. 10.9). Four transects of point spectra additionally indicate that the Fe content typically varies in the rhombs, with the cores in Fig. 10.9a and c being non-ferroan, their rims ferroan. High Mg content is characteristic of the rhombs, with lower values occasionally found toward the rims. The enclosing late-stage calcite is non-ferroan, and similarly contains minimal Mg. Pitted rhombs, particularly the one shown in Fig. 10.9b, have higher levels of impurities than pure rhombs, suggesting encapsulation of aluminum silicates

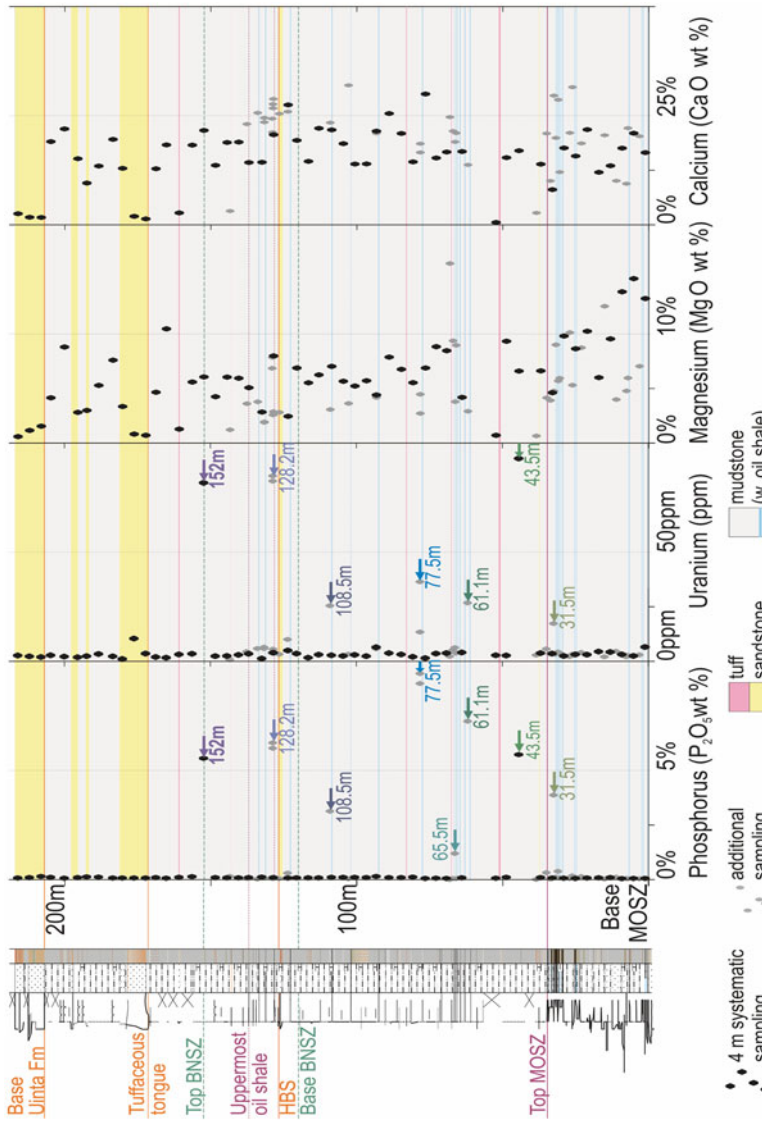

Fig. 10.5 Raw wt% as oxide and ppm data for various elements as determined from ICP analysis of samples from the upper GRF at Buck Canyon. Data from the systematic sampling, every 4 m, is shown by *black diamonds*. Additional (focussed) sampling of selected beds are shown by *gray diamonds*. The relative standard deviation from replicate analyses is <5 % for major elements and <10 % for the minor element, and uncertainty associated with various determinations is ±15 % at ten times, and ±5 % at 100 times the detection limits (limits: P_2O_5, CaO, MgO = 0.01 %; U = 0.1 ppm)

Table 10.2 XRD Analyses of 9 samples from the BNSZ of the upper GRF at Buck Canyon

Sample Horizon	Lithofacies	Quartz	Feldspar	Mica	Calcite	Dolomite	Zeolite	Phosphate
152 m	2	15	11	–	19	38	2	15
144 m	2	11	21	6	21	41	–	–
140 m	2	14	21	–	28	37	–	–
137.2 m	1	12	14	–	40	35	–	–
133.5 m	1	10	13	–	56	21	–	–
131 m	1	11	16	14	33	26	–	–
128.2 m	1	16	30	–	33	3	–	18
128.1 m	1	1	14	–	58	27	–	–
126 m	3	29	14	–	28	29	–	–

The reference-intensity-ratio method was used to estimate the weight fractions of the different phases. Errors are generally ±5 %, but increase with more diverse sample mineralogy, lower abundance of a mineral, overlapping peaks, and increasing presence of clays and salts

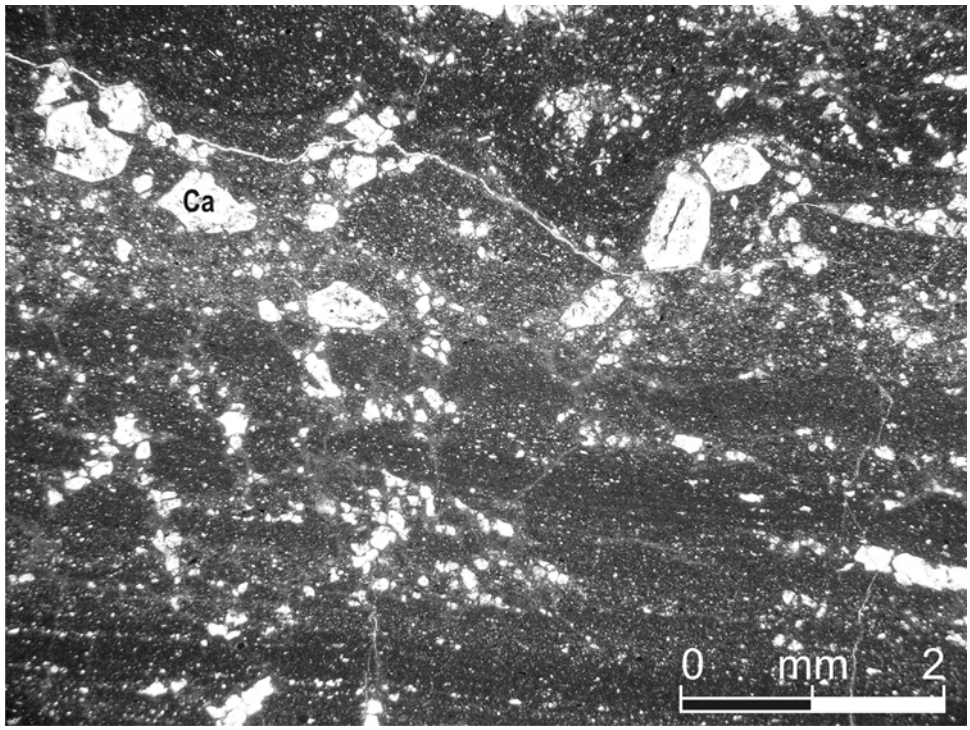

Fig. 10.6 Thin section photomicrograph of the carbonate shale at 152 m exhibits a lamination disrupted by variably sized nodules and microfractures. The shape of several crystals is closer to the form of shortite, suggesting the calcite (Ca) now present is a pseudomorphic phase. The original mineral is considered to have grown in situ because of the numerous inclusions of carbonate shale still embedded in the crystal form

by the growing dolomite crystal. Where P is recorded (e.g., rhombs in Fig. 10.9b, c) it occurs adjacent to the dolomite–calcite contact, or even enclosing the dolomite rhombs (Fig 10.9b). EDS data provide ambiguous evidence as to whether the P represents the element substituting in the carbonate lattice or that the calcite grew around and enveloped microcrystalline CFA.

10.7 Interpretations

10.7.1 Depositional Environments of the BNSZ

Facies models of evaporative lakes (e.g., Renaut and Gierlowski-Kordesch 2010) consider irregular and discontinuous, displacive and often pseudomorphed crystals in weakly laminated mudstone to form marginally, such as within saline mudflats during lake regressions, with cumulative, bedded evaporites typically forming near the basin/lake center. This model is appropriate for the BNSZ. In Buck Canyon, the lower and upper saline intervals (lithofacies 2c) are of a very limited thickness and identified only by pseudomorphing calcite crystals disrupting (brecciating) bedding (e.g., 152 m), suggesting a marginal setting. In the upper saline zone, interbedded lithofacies 2b may provide another indication of shallow water conditions. Lenticular cracks in the GRF have previously been considered related to subaqueous physical stresses associated with wave activity (Picard 1966; "diastasis" of Cowan and James 1992). However, subaqueous salinity changes affecting muds containing minor quantities of swelling clays ("synaeresis" of Plummer and Gostin 1981) cannot be ruled out. In strata below 152 m, the association of diagenetic pyrite (outcrop only) indicates that low Eh porewaters containing abundant dissolved ferrous iron and sulfide were present in the substrate (Hesse 1990) but not necessarily that the shallow lake waters were anoxic. The two saline intervals are considered to represent lateral facies transitions from the nodular nahcolite beds (Keighley 2013). Bedded nahcolite nodules increase in size and occur over greater stratal thicknesses toward the northeast, which indicates the direction to the evaporitic lake depocenter (Cashion 1967; Vanden Berg et al. 2013).

In the broader picture, occurrences of lithofacies 1 and its components within the BNSZ of Buck Canyon are interpreted as lateral facies extensions of the middle R-8 zone of the cores, and to represent anoxic-lake highstands (Desborough 1978). Interbeds of lithofacies 2a, and lithofacies 2 in general, ambiguously record either more oxic lake conditions that allowed for the breakdown of organic detritus or a lower productivity lake that might have existed under the saline conditions. The high carbonate content of the interbedded lithofacies 1 and 2 successions indicates a mostly clastic-starved setting, likely an offshore location.

Lithofacies 3b in the HBS exhibits a coarsening upward profile that, together with the contained wave-influenced sedimentary structures, indicates a prograding shoreface. The HBS thickens westward, where planar cross-strata additionally interbed to indicate a fluvio-deltaic source for the shoreface sandstone. Lying within the BNSZ, the HBS has previously been interpreted to be a lake low-stand succession (Brownfield et al. 2010) although at a higher resolution, it lies stratigraphically between two oil shale beds (lithofacies 1) and so could be considered a stand-still deposit during the transgressive phase that followed deposition of the lower saline interval.

In summary, although there was an overall trend upsection from an anoxic, balanced-fill, deep lake during deposition of the MOSZ to a predominantly underfilled, restricted evaporative basin during deposition of the BNSZ, lake transgressions and anoxic deep lake conditions still occurred periodically (i.e., the cyclicity noted by Smith et al. 2008). Within this context, the BNSZ at Buck Canyon would occupy a proximal position to the southerly, fluctuating but mostly closed-lake shoreline and to have formed during prolonged regressive lake stages as quiet, shallow water deposits close to marginal mud-flats. The P-enriched bed at 152 m is equated with a prolonged saline event accompanying a lake low stand.

10.7.2 Cause of Phosphorus Anomalies in the BNSZ

The basic P cycle for lakes is reviewed in detail elsewhere (e.g., Föllmi 1996; Wetzel 2001, and see Fig. 10.10) but usually the cycle leads to the epilimnion becoming a major P sink. Reserves of available P in the epilimnion are ultimately

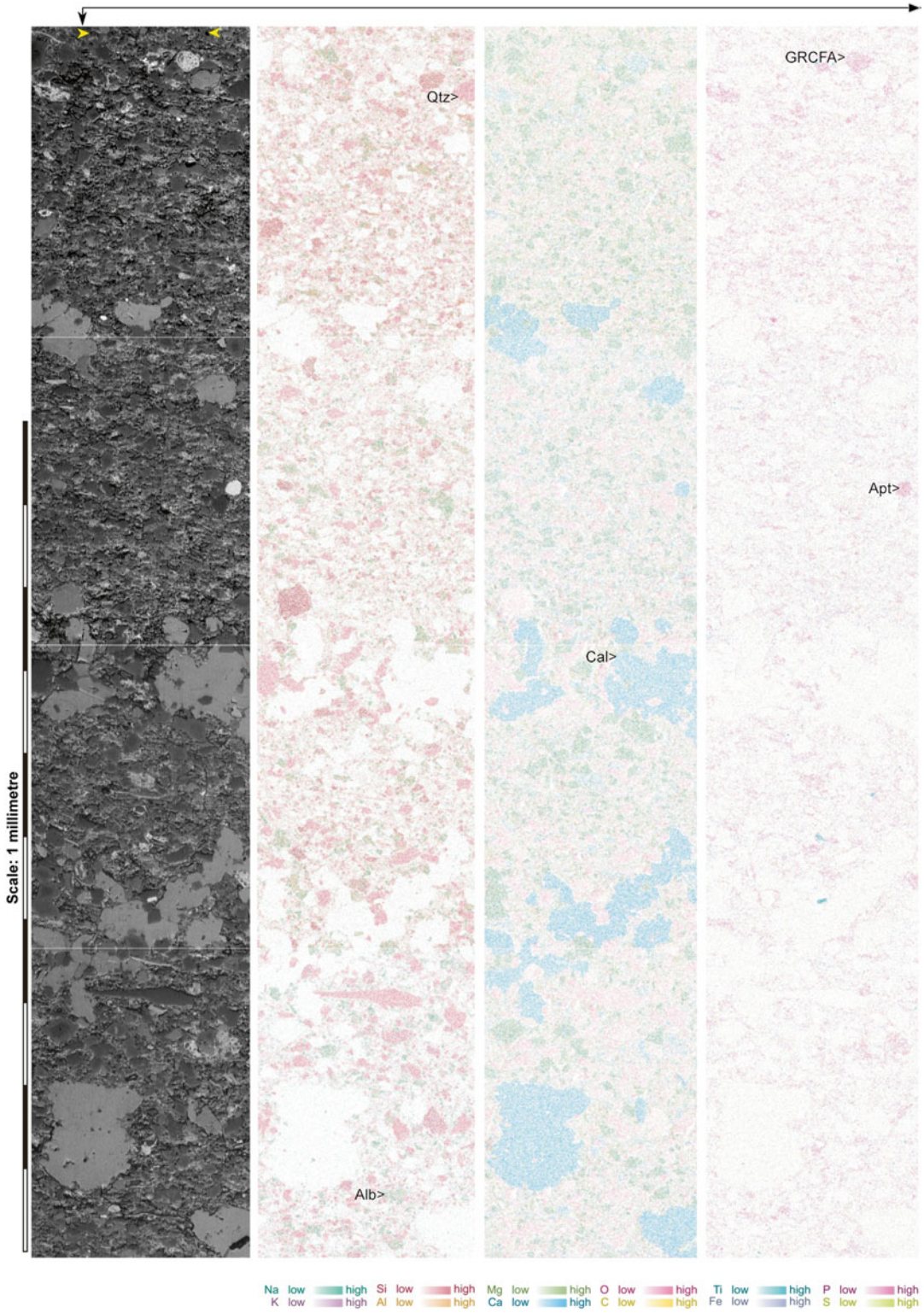

Fig. 10.7 SEM images of the carbonate shale at 152.0 m. For each sample, the first column is a montage of Back-Scattered Electron (BSE) images, with the other three columns being color-coded maps for selected elements to give a general indication of sample mineralogy. *Alb* albite, *AlkF* alkali feldspar, *Apt* apatite (detrital grain), *Cal* calcite, *Dol* dolomite, *GRCFA* grain-replacive calcium fluorapatite, *Qtz* quartz, *RFF* resin-filled fracture, *Rut* rutile, *ShS* sheet silicate

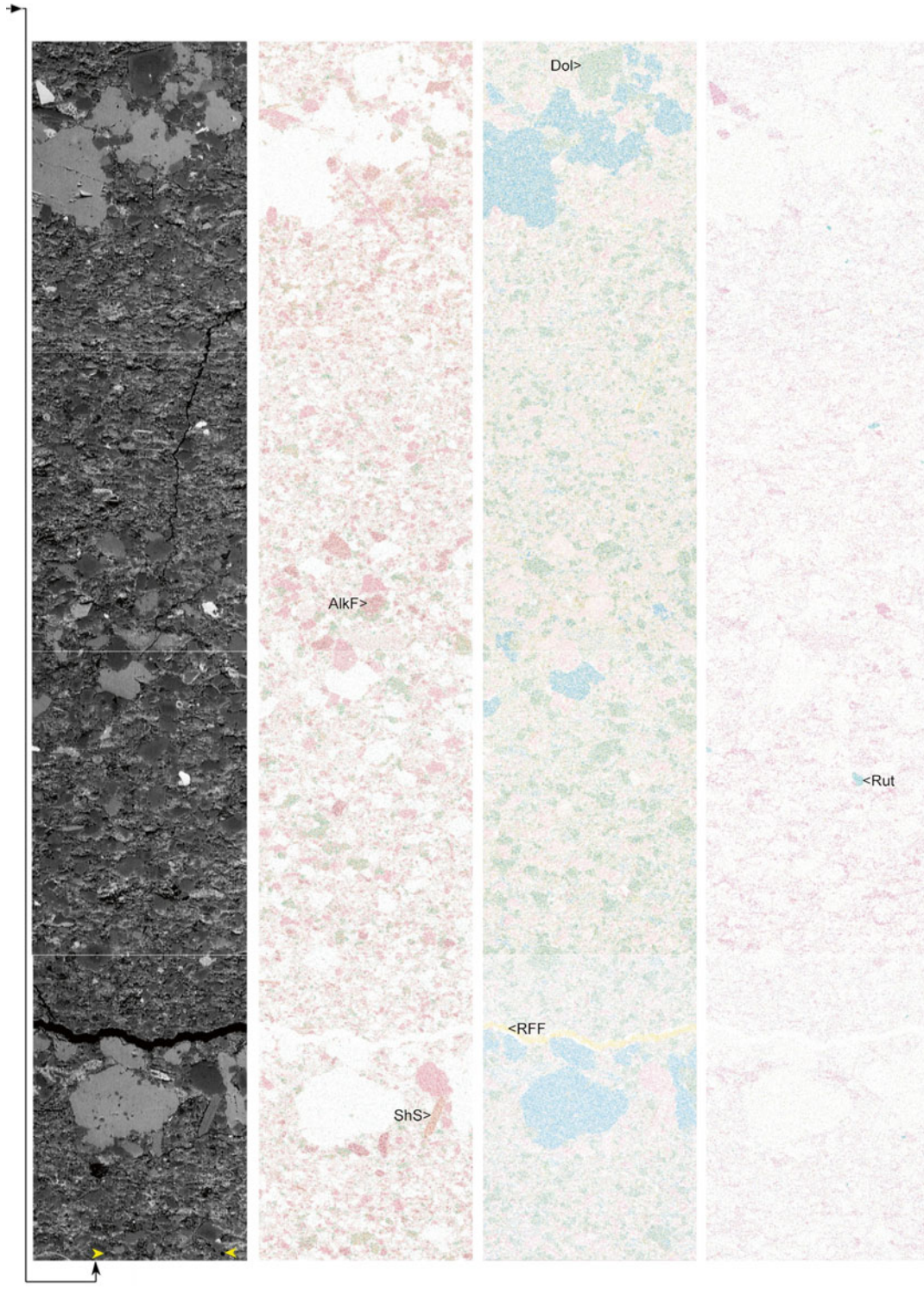

Fig. 10.7 (continued)

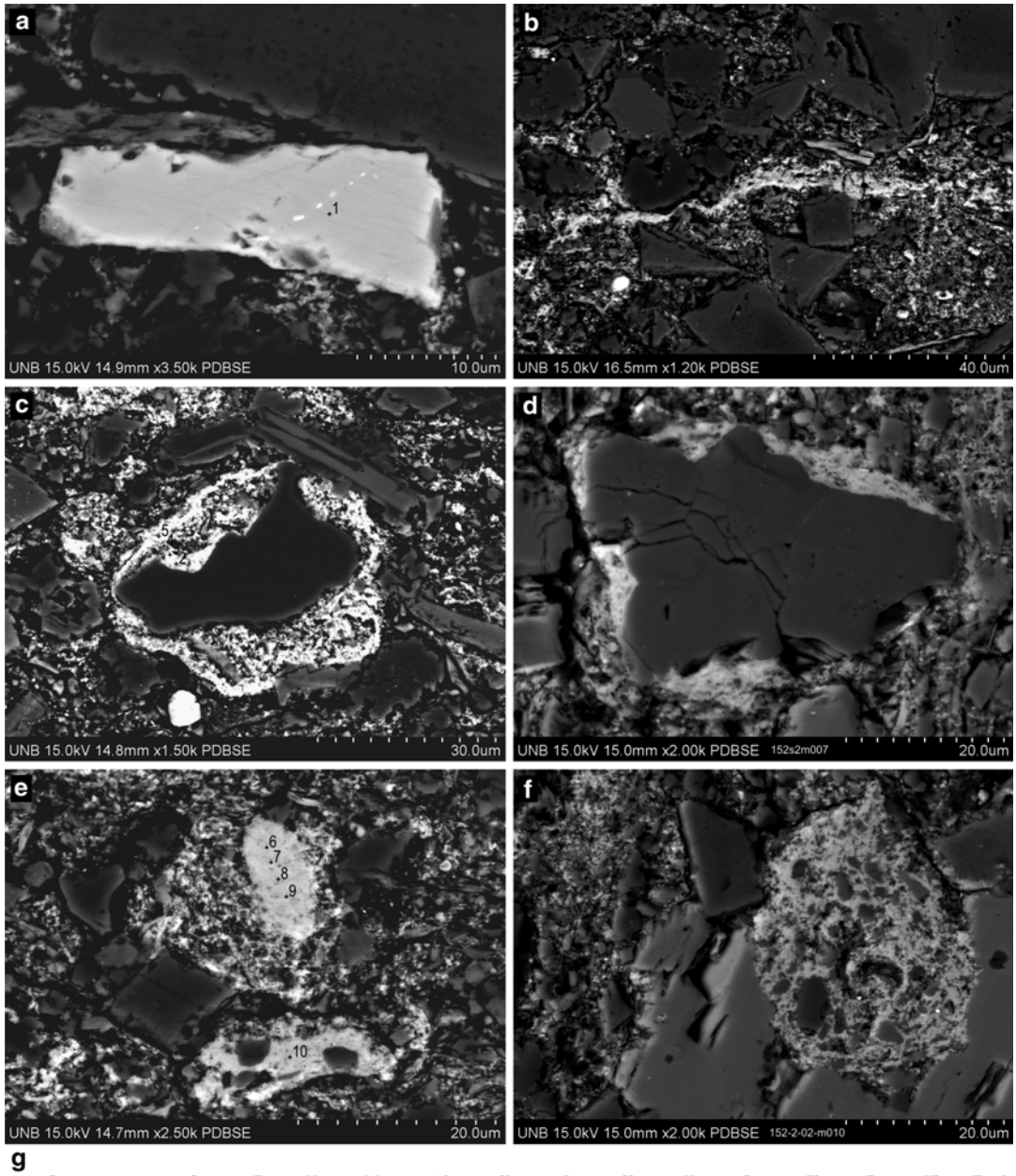

g

Spectrum	O	F	Na	Mg	Al	Si	P	Cl	K	Ca	Ti	Fe	Yb	Total
Spectrum(1)	39.12	7.87					19.90	0.20		38.25		0.26	0.00	105.59
Spectrum(2)	29.41	4.11	0.68	0.58	1.14	4.71	15.32		0.67	30.79	0.90	0.75		89.06
Spectrum(3)	40.45	4.94	0.81	1.54	2.33	8.58	14.90		1.21	28.11		1.14		104.01
Spectrum(4)	21.41	1.83	0.45	1.08	1.44	7.81	13.22		1.00	26.05	0.23	1.27		75.80
Spectrum(5)	27.59	3.31	0.62	1.11	1.65	7.15	15.71		0.89	27.79		1.08		86.90
Spectrum(6)	10.72	1.33	0.33	0.16	0.19	0.98	16.42		0.24	31.15		0.39	0.00	61.91
Spectrum(7)	40.16	5.68	1.14	0.48	0.43	1.96	17.02			33.93				100.79
Spectrum(8)	8.51	1.07	0.30	0.12	0.61	3.37	15.10		0.53	27.86		0.40		57.88
Spectrum(9)	7.98	0.91	0.20	0.10	0.15	0.83	14.11		0.22	28.57		0.47	0.00	53.53
Spectrum(10)	16.72	2.06	0.59	0.35	0.75	2.94	16.58		0.56	30.86		0.74		72.15

depleted only when the P-bearing dead biota is able to permanently sink down through the hypolimnion in stratified (meromictic) lakes (Levine et al. 1986). The biotic detritus is then able to settle out onto the substrate, to join detrital inorganic P phases and phases precipitated from solution (gross P sedimentation). Ultimately the detritus and P is buried and lithified in the sediment pile prior to later uplift for renewed weathering. However, a major complication to the cycle exists because, even after initial sedimentation, P may recycle back into the hypolimnion by remobilization from particulate stores into dissolved interstitial P by various mechanisms under anaerobic conditions (Boström et al. 1988; and discussed below). Where there is no well-established and permanent hypolimnion, a significant P-concentration gradient can then be present between the interstital and lake waters, promoting molecular diffusion into the overlying water column (gross P release). From a steady-state viewpoint, P retention (net P sedimentation) = gross P sedimentation – gross P release (Hupfer and Lewandowski 2008). For much of the BNSZ, ICP analyses (Fig. 10.5) indicate low background P concentrations and hence gross P sedimentation ≥ gross P release. Exceptionally, the sample from 152 m indicates a situation where gross P sedimentation ≫ gross P release. As reviewed earlier, such enrichment is rare in the known lacustrine geologic record and requires an explanation.

Temporary increased net P sedimentation may result from increased gross P sedimentation and, or, reduced gross P release. For the 152 m sample, increases in gross P sedimentation do not appear to be directly responsible for several reasons. Even though the drainage basin would have included apatite-bearing outcrops of the Phosphoria Formation (e.g., Hendrix and Byers 2000) and fresh volcanic ash falls (e.g., Smith et al. 2008), refractory P-bearing grains are rare (Fig. 10.7). Although outcrop is poor, carbonate shale overlies the phosphatic bed, so there is no evidence for increased dissolved-P influx via deposition of overlying tuffaceous or coarse clastic layers (Fig. 10.3). Also absent are skeletal hard parts and evidence of hardground reworking: the bed can be considered a "pristine phosphate" (Föllmi 1996). Gross P sedimentation may well have been enhanced by way of influxes of adsorbed inorganic-P on calcite or clays such as smectite (e.g., Ruttenberg and Berner 1993; Song et al. 2006; Holmkvist et al. 2010). Detrital Fe-oxides are absent from the strata and are unlikely to have been a common source of adsorbed P because the BNSZ was deposited when Lake Uinta likely had predominantly high pH, and sorption capacities for Fe-oxides decrease as pH levels increase above 6.5 (Stumm and Morgan 1996) and in the presence of dissolved sulfate (Katsev et al. 2006). Most importantly, the element is not present in its original organic or adsorbed inorganic phosphate phase, but as crystalline (precipitated) CFA.

Love (1964) and Swirydczuk et al. (1981) have proposed that phosphates in ancient lakes in Utah could have precipitated directly from periodically highly stratified hypersaline water columns (e.g., caused by a sudden drying of the

Fig. 10.8 Detailed BSE images with selected EDS analyses of CFA phases from 152 m. (**a**) Possibly an angular detrital grain of relatively pure CFA (Cl can substitute for F in the CFA lattice). (**b**) Ca and P are mapped as variably abundant in the matrix, and can concentrate (*brighter gray* – reflecting elements with higher atomic number) along irregular stringers, possibly related to precursor organic-rich laminae. (**c**, **d**) Variably thick coatings of sub-micron-scale crystals (EDS indicates an admixture of clays and/or carbonates, and CFA: the complexity of the matrix makes definitive EDS analysis of the CFA composition problematic due to limitations in the focus and penetration of the electron beam), each surrounding a silicate grain. (**e**) Variably dense, somewhat fibrous microcrystalline CFA and admixed clay/silicate/carbonate that may itself be diagenetic replacement or residual material of a precursor grain. The CFA bottom center may be replacing the groundmass of a multi-minerallic grain. (**f**) Another potentially phosphatized multi-mineralic grain is mostly enclosed by late-stage pseudomorphic calcite exhibiting the highly pitted morphology typical of this phase. (**g**) Tabulation of EDS spot analyses located in 8a, c, and e

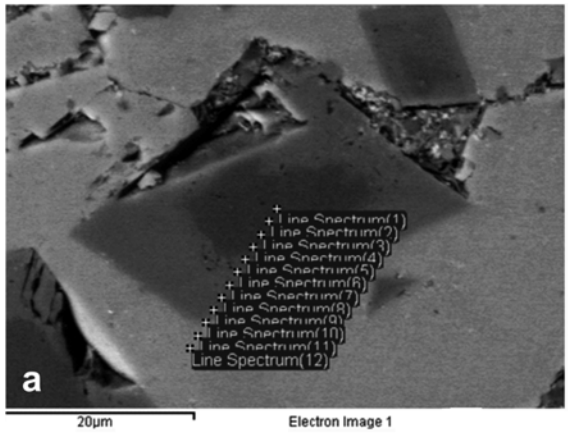

SAMPLE 152A

Spectrum	Mg	Ca	Fe	O	Al	Si	Na	K	Mn	P	Total
Line Spectrum(1)	11.23	21.41		29.80							62.44
Line Spectrum(2)	11.96	21.55		27.73							61.24
Line Spectrum(3)	11.82	21.41	0.39	27.32							60.94
Line Spectrum(4)	11.95	21.98	0.87	27.53					0.19		62.51
Line Spectrum(5)	5.63	20.48	2.12	11.69					0.18		40.10
Line Spectrum(6)	7.85	22.09	2.10	21.08	0.14	0.31					53.57
Line Spectrum(7)	10.36	23.59	2.83	27.40							64.17
Line Spectrum(8)	9.61	24.69	2.89	25.14							62.33
Line Spectrum(9)	5.22	29.97	2.28	14.26							51.72
Line Spectrum(10)	4.86	35.68	1.87	30.71							73.12
Line Spectrum(11)	0.21	32.66	0.42	14.22							47.52
Line Spectrum(12)	0.17	40.22	0.26	23.32							63.98
Max.	*11.96*	*40.22*	*5.27*	*30.71*	*0.14*	*0.31*			*0.19*		
Min.	*0.17*	*20.48*	--	*11.69*	--	--			--		

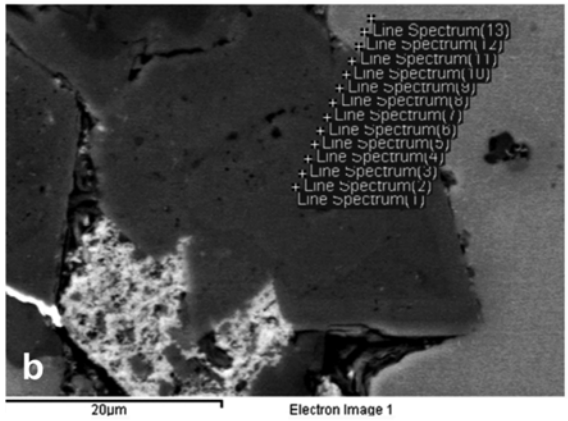

SAMPLE 152B

Spectrum	Mg	Ca	Fe	O	Al	Si	Na	K	Mn	P	Total
Line Spectrum(1)	9.09	20.18	4.22	18.42							51.91
Line Spectrum(2)	5.30	19.61	3.68	13.00		0.11					41.70
Line Spectrum(3)	9.85	21.92	4.29	19.07			0.11				55.25
Line Spectrum(4)	4.56	20.83	2.67	8.84	0.10	0.50					37.49
Line Spectrum(5)	8.39	21.47	1.76	19.97		0.19			0.23		52.01
Line Spectrum(6)	7.71	21.27	1.04	18.31							48.34
Line Spectrum(7)	12.12	23.82	2.14	31.07							69.15
Line Spectrum(8)	6.08	20.99	2.85	11.47		0.11					41.50
Line Spectrum(9)	7.27	24.04	2.62	19.21	0.33	1.45		0.25	0.18	0.67	56.01
Line Spectrum(10)	3.26	32.71	1.69	34.44	1.55	4.36		0.28		0.73	79.03
Line Spectrum(11)	0.15	34.17	0.34	13.37		0.16				0.12	48.30
Line Spectrum(12)	0.11	31.99	0.48	12.76		0.10				0.18	45.63
Line Spectrum(13)		27.24	0.31	8.02		0.14				0.20	35.90
Max.	*12.12*	*34.17*	*4.29*	*34.44*	*1.55*	*4.36*	*0.11*	*0.28*	*0.23*	*0.73*	
Min.	--	*19.61*	*0.31*	*8.02*	--	--	--	--	--	--	

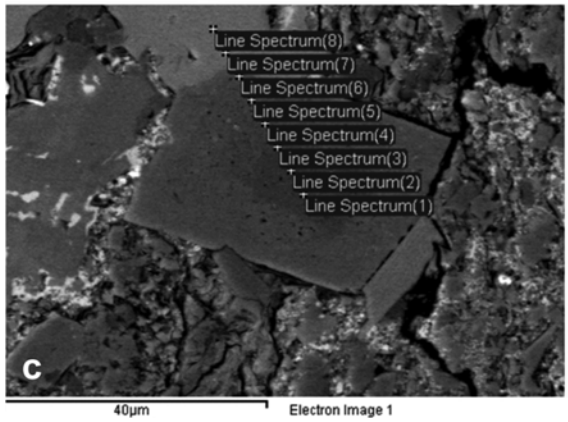

SAMPLE 152C

Spectrum	Mg	Ca	Fe	O	Al	Si	Na	K	Mn	P	Total
Line Spectrum(1)	4.60	17.67	0.28	13.16							35.70
Line Spectrum(2)	8.44	20.24		22.06							50.74
Line Spectrum(3)	3.72	17.14	1.07	5.98		0.12			0.46		28.48
Line Spectrum(4)	6.99	19.53	1.95	13.52					0.23		42.21
Line Spectrum(5)	5.07	18.83	2.75	11.12							37.77
Line Spectrum(6)	5.00	21.46	3.41	14.85						0.79	45.51
Line Spectrum(7)	0.16	37.07		23.24							60.47
Line Spectrum(8)		33.75	0.26	18.51							52.53
Max.	*8.44*	*37.07*	*3.41*	*23.24*		*0.12*			*0.46*	*0.79*	
Min.	--	*17.14*	--	*5.98*		--			--	--	

Fig. 10.9 BSE images and tabulated EDS analyses from 152 m detailing the zoning and diagenetic relationships in carbonates. (**a**) The EDS analyses are from a transect that runs from a core of NF dolomite through zoned Fe dolomite and out into late stage calcite. (**b**) A zoned Fe dolomite is post-dated by bright CFA microcrystalline aggregates (*lower left*) and large blocky calcite (*right*). Note that P is recorded only in the outermost five spectra, further indicating that the core had precipitated prior to P coming out of solution. (**c**) The EDS analyses again indicate a zoned dolomite, non-ferroan at its core with P recorded close to the rim (spectrum 6) and the contact with the low-Mg calcite (spectra 7 and 8). All results in weight percent. Processing option: all elements analyzed (values for carbon omitted: sample was carbon coated)

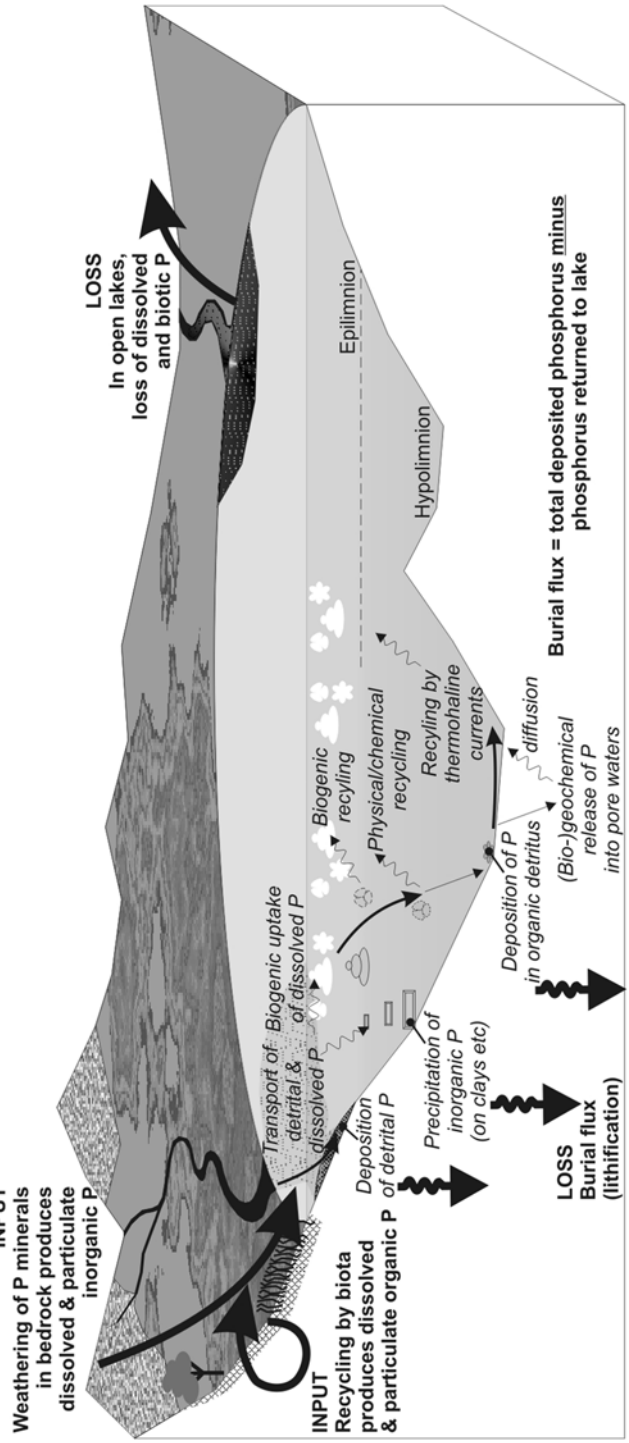

Fig. 10.10 The phosphorus cycle in lakes (Adapted from Keighley 2013)

climate) with the development of a chemocline that could act as a phosphate trap, inhibiting recycling into surface waters. However, in this sample the CFA is considered diagenetic because (i) settling of precipitated platy crystals in a low-energy environment would be expected to impart a preferred orientation, (ii) localized concentration of CFA as grain coatings, and (iii) P is recorded in SEM at the contact between authigenic dolomite and later calcite. The chemocline simply may have limited upward diffusion gradients, allowing P to accumulate and reach saturation in substrate pore waters.

Increased net P sedimentation is therefore considered the result of lowered gross P release due to initial substrate remobilization, by methods outlined in Boström et al. (1988), followed by its precipitation as diagenetic CFA. Jahnke (1984) and Van Cappellen and Berner (1988, 1991) identify CFA as the thermodynamically stable apatite phase that precipitates early and rapidly from high-carbonate, high pH solutions in the very shallow substrate. It remains uncertain whether CFA precipitates directly, or via precursor phosphate-mineral phases (e.g., Emerson 1976; House 1999; Song et al. 2002), or as a phosphatic gel (e.g., Slansky 1986).

As noted by Van Cappellen and Berner (1991) for oceans, and for example Kleeberg and Dudel (1997) and Anshumali (2007) for geochemically more variable lakes, the kinetics of apatite precipitation are influenced by numerous interlinked controlling parameters including dissolved-ion abundance (NO_3^-, CO_3^{2-} SO_4^{2-}, O^{2-}) and dissolved organic molecules, as well as temperature, salinity, alkalinity, pH, and Eh. Furthermore, redox reactions, adsorption, mineral phase solubility, and mineralization of organic matter are all mechanisms that have been invoked for bringing the primary CFA ions (F, Ca, and PO) to concentrations probably well above equilibrium (Knudsen and Gunter 2002). None of these mechanisms is universally dominant (e.g., Van Cappellen and Berner 1991; Kaiserli et al. 2002; Katsev et al. 2006) and, in particular, the long-held paradigm that redox, particularly involving Fe-oxides, is the major mechanism has now been shown to be valid only under special circumstances for lakes (Hupfer and Lewandowski 2008).

If all major components of CFA were at saturation, the main limiting control would have been the presence of Mg^{2+} in solution. At neutral pH, CFA growth is limited if the Ca:Mg ratio drops below 1.2:1, but at a pH of 7.5–8, CFA is limited if the ratio drops below 5.2:1 (Knudsen and Gunter 2002). The Mg^{2+} ion either may be incorporated into the apatite crystal, resulting in lattice distortion that limits crystal growth (Gulbrandsen et al. 1984), or the Mg^{2+} may block crystal growth sites simply by its adsorption onto the crystal (Van Cappellen and Berner 1991). High Ca:Mg ratios can be attained by removal of Mg^{2+}, by enrichment of Ca^{2+}, such as by dissolution of calcite or gypsum (Nathan and Lucas 1972), or by authigenesis. The diagenetic succession of phosphate post-dating the abundant rhombic dolomite crystals (Fig. 10.9) suggests that only once the Mg^{2+} was incorporated into the dolomite cement in the substrate – this reaction also liberates F^- ions from MgF complexes, aiding fluoride saturation – could phosphogenesis commence.

The dolomite in question can be considered a primary, penecontemporaneous dolomite, and its rhombic form directs interpretation toward the evaporative pumping sabkha model of dolomite formation (Morrow 1990). Even so, dolomite precipitation is itself problematic, with poorly understood kinetic effects where there are temperatures below 50 °C and low dissolved sulfate (e.g., Machel 2004; Armenteros 2010). The formation of nahcolite, rather than the trona common in the Wyoming lakes, suggested to Milton and Eugster (1959) that moderate lake temperatures of 35 °C or less persisted in the possibly deeper water Uinta Basin (lower with higher atmospheric CO_2: Lowenstein and Demicco 2006). However, despite low sulfate concentrations in Lake Uinta, if any organic matter was breaking down in the substrate, the presence of methanogenic bacteria may have promoted progressively Fe-enriched dolomites with biogenic sulfate reduction being suppressed (Mazzullo 2000). The lack of pyrite at 152 m is further support. Whereas Fe^{2+} was forming from the breakdown of limited

Fe-silicates, oxides, and highly reactive organic iron compounds by Fe-reducing bacteria, any H_2S that was generated slightly deeper in the substrate and that diffused upward would be kinetically inhibited from reacting with the Fe^{2+} due to high porewater pH (Tuttle and Goldhaber 1993). Iron was thus increasingly available for incorporation into a dolomite lattice provided methanogenesis maintained high pH and carbonate alkalinity (Mazzullo 2000).

The localized concentration of CFA as grain coatings and partial grain replacements (Fig. 10.8) suggests they were the preferred CFA nucleation sites. Both Mg-bearing smectite and zeolite are considered effective adsorption sites for P (e.g., Ruttenberg and Berner 1993; Sakadevan and Bavor 1998; Stamatakis and Koukouzas 2001), and their precipitation as clay rims or partial alterations of volcanic grains could also have contributed to lower Mg^{2+} levels. Authigenic zeolite and smectite can form by evaporative pumping around volcanic-influenced saline lake margins (e.g., Renaut 1993; Hay and Kyser 2001). Smectite has not been verified either in XRD or SEM for this sample, but was noted in the upper GRF further east by Dyni (1976) and Bristow et al. (2012) who found that dolomite abundance was related to the inverse of Mg-smectite abundance.

10.8 Conclusions

Low background concentrations of P are recorded from ICP analyses of 89 samples from the upper GRF of the Uinta Basin, Utah, and indicate that a minor amount of phosphate was continuously accumulating during the deposition of over 200 m of Eocene lacustrine strata. However, in the BNSZ one carbonate shale containing calcite pseudomorphs (as well as an oil shale bed not detailed herein), phosphorus peaks at values of over 5 wt% of the oxide. XRD analysis of 9 samples from the BNSZ confirms CFA as the major P-bearing mineral. Thin section and SEM observations identify the CFA as microcrystalline aggregates, with EDS recording the presence of sodium and sulfate that would have substituted into the CFA crystal lattice. Diagenetic calcite is considered to pseudomorph large shortite crystals as well as to enclose rhombic zoned ferroan dolomite in precipitate-dominated laminae.

The establishment of a chemocline in a high pH, high alkalinity, saline lake of low organic productivity may have caused dissolved P to reach saturation in lake and pore waters. However, CFA would not normally precipitate because at high pH, Mg^{2+} in solution effectively inhibits CFA precipitation. Evaporative pumping to the adjacent sabkha, potentially also with the activity of methanogenic bacteria, led to the precipitation of rhombic, zoned ferroan dolomite, reducing dissolved Mg^{2+} content, and permitting CFA to then precipitate, possibly also in association with smectite diagenesis.

Acknowledgments Manuscript reviewers and editors provided detailed and constructive comments. D. MacIsaac assisted with logging and sampling. V. Reddy (UNB Earth Sciences) undertook the XRD analyses. Sample chips and thin sections were produced by A. Murphy and C. Nash (UNB Earth Sciences). SEM analysis was courtesy of S. Boonsue and J. Spray (UNB Earth Sciences). Field and stratigraphic discussions with M. Vanden Berg, D. Sprinkel and C. Morgan (Utah Geological Survey) were very constructive. Funding for this project was provided in part by an NSERC Discovery Grant and by a Utah Geological Survey, State of Utah Petroleum Research Grant.

References

Anshumali RAL (2007) Phosphorus fractionation in surficial sediments of Pandoh Lake, Lesser Himalaya, Himachal Pradesh, India. Appl Geochem 22:1860–1871

Armenteros I (2010) Diagenesis of carbonates in continental settings. In: Alonzo-Zarza AM, Tanner LH (eds) Carbonates in continental settings: geochemistry, diagenesis and applications, vol 62, Developments in sedimentology. Elsevier Science, Amsterdam/London, pp 61–151

Bein A (1986) Stable isotopes, iron and phosphorus in a sequence of lacustrine carbonates – paleolimnic implications. Chem Geol 59:305–313

Birgenheier LP, Vanden Berg MD (2011) Core-based integrated sedimentologic, stratigraphic, and geochemical analysis of the oil shale bearing Green River Formation, Uinta Basin, Utah. United States Department of Energy and National Energy Technology Laboratory, Topical report, 19 p

Boström B, Andersen JM, Fleischer S, Jansson M (1988) Exchange of phosphorus across the sediment-water interface. Hydrobiologia 170:229–244

Bradley WH (1929) The occurrence and origin of analcite and meerschaum beds in the Green River Formation of Utah, Colorado, and Wyoming, U.S. Geological Survey, professional paper 158-A. U.S. Government Printing Office, Washington, DC, p 7

Bradley MD (1995) Timing of the Laramide rise of the Uinta Mountains, Utah and Colorado. In: Jones RW (ed) Resources of Southwestern Wyoming. Wyoming Geological Association, Casper, Wy, pp 31–44

Bristow TF, Kennedy MJ, Morrison KD, Mrofka DD (2012) The influence of authigenic clay formation on the mineralogy and stable isotopic record of lacustrine carbonates. Geochim Cosmochim Acta 90:64–82

Brownfield ME, Johnson RC, Dyni JR (2010) Sodium carbonate resources of the Eocene Green River Formation, Uinta Basin, Utah and Colorado. U.S. Geological Survey, Digital data series DDS-69-BB, Ch. 2, 13 p

Carasco B (1989) Lacustrine sedimentation in a Permian intermontane basin: the Villé Graben (Vosges, France). Palaeogeogr Palaeoclimatol Palaeoecol 70:179–186

Cashion WB (1967) Geology and fuel resources of the Green River Formation, southeastern Uinta Basin, Utah and Colorado, vol 548, U.S. Geological Survey, professional paper. U.S. Government Printing Office, Washington, DC, p 48

Cashion WB (1995) Stratigraphy of the Green River Formation, eastern Uinta Basin, Utah and Colorado—a summary. In: Averett WR (ed) The Green River Formation in Piceance Creek and Eastern Uinta Basins field trip 1995. Grand Junction Geological Society, Grand Junction, Co, pp 15–21

Cowan CA, James NP (1992) Diastasis cracks: mechanically generated synaeresis-like cracks in Upper Cambrian shallow water oolite and ribbon carbonates. Sedimentology 39:1101–1118

Dane CH (1954) Stratigraphic and facies relationships of the upper part of the Green River Formation and lower part of the Uinta Formation in Duchesne, Uintah, and Wasatch counties, Utah. AAPG Bull 38:405–425

De las Heras X, Grimalt JO, Albaigés J (1989) Origin and diagenesis of the organic matter in Miocene freshwater lacustrine phosphates (Cerdanya Basin, eastern Pyrenees). Org Geochem 14:667–677

Desborough GA (1978) A biogenic-chemical stratified lake model for the origin of oil shale of the Green River Formation: an alternative to the playa-lake model. Geol Soc Am Bull 89:61–971

Desborough GA, Pitman JK, Hufman C (1976) Concentration and mineralogical residence of elements in rich oil shales of the Green River Formation, Piceance Creek Basin, Colorado, and the Uinta Basin, Utah – a preliminary report. Chem Geol 17:13–26

Dickinson WR, Klute MA, Hayes MJ et al (1988) Paleogeographic and paleotectonic setting of Laramide sedimentary basins in the central Rocky Mountain region. Geol Soc Am Bull 100:1023–1039

Dietrich R (1978) Das Messelitproblem: Messelit und Anapait aus dem Olschiefervorkommen bei Messel. Der Aufschluss Sonderheft 29:229–233

Donnell JR (2009) Intertonguing of the lower part of the Uinta Formation with the upper part of the Green River Formation in the Piceance Creek Basin during the late stages of Lake Uinta. U.S. Geological Survey, scientific investigations report 2008–5237, 25 p

Dyni JR (1976) Trioctahedral smectite in the Green River Formation, Duchesne County, Utah, vol 967, U.S. Geological Survey, professional paper. U.S. Government Printing Office, Washington, DC, p 14

Dyni JR (1996) Sodium carbonate resources of the Green River Formation, U.S. Geological Survey, open-file report 1996–729. U.S. Dept. of the Interior, U.S. Geological Survey, Denver, p 39

Emerson SE (1976) Early diagenesis in anaerobic lake sediments: chemical equilibria in interstitial waters. Geochim Cosmochim Acta 40:925–934

Fabbi BP, Espos LF (1976) X-ray fluorescence analysis of 21 selected major, minor, and trace elements in eight new USGS standard rocks. In: Flanagan FJ (ed) Description and analyses of eight new USGS rock standards, vol 840, U.S. Geological Survey, professional paper. U.S. Dept. of the Interior, U.S. Geological Survey, Reston, p 192

Fahey JJ (1962) Saline minerals of the Green River Formation, vol 405, U.S. Geological Survey, professional paper. U.S. Government Printing Office, Washington, DC, p 50

Föllmi KB (1996) The phosphorus cycle, phosphogenesis and marine phosphate-rich deposits. Earth-Sci Rev 40:55–124

Gromet LP, Dymek RF, Haskin LA, Korotev RL (1984) The "North American Shale Composite": its compilation, major, and trace element characteristics. Geochim Cosmochim Acta 48:2469–2482

Gulbrandsen RA, Robertson CE, Neil ST (1984) Time and crystallization of apatite in seawater. Geochim Cosmochim Acta 48:213–218

Hay RL, Kyser TK (2001) Chemical sedimentology and paleoenvironmental history of Lake Olduvai, a Pliocene lake in northern Tanzania. Geol Soc Am Bull 113:1505–1521

Hendrix MS, Byers CW (2000) Stratigraphy and sedimentology of Permian strata, Uinta Mountains, Utah: allostratigraphic controls on the accumulation of economic phosphate. In: Glenn CR, Prévôt-Lucas L, Lucas J (eds) Marine authigenesis: from global to microbial, vol 66, SEPM Special Publication. SEPM (Society for Sedimentary Geology), Tulsa, pp 349–367

Hesse R (1990) Early diagenetic pore water/sediment interaction: modern offshore basins. Geosci Canada Reprint Ser 4:277–316

Holmkvist L, Arning ET, Küster-Heins K et al (2010) Phosphate geochemistry, mineralization processes, and *Thioploca* distribution in shelf sediments off central Chile. Mar Geol 277:61–72

House WA (1999) The physico-chemical conditions for the precipitation of phosphate with calcium. Environ Technol 20:727–733

Hupfer M, Lewandowski J (2008) Oxygen controls the phosphorus release from lake sediments – a long-lasting paradigm in limnology. Int Rev Hydrobiol 93:415–432

Jahnke RA (1984) The synthesis and solubility of carbonate fluorapatite. Am J Sci 284:58–78

Johnson RC (1981) Stratigraphic evidence for a deep Eocene Lake Uinta, Piceance Creek Basin, Colorado. Geology 9:55–62

Kaiserli A, Votusa D, Samara C (2002) Phosphorus fractionation in lake sediments – Lakes Volvi and Koronia, N. Greece. Chemosphere 46:1147–1151

Katsev S, Tsandev I, L'Heureux I, Rancourt DG (2006) Factors controlling long-term phosphorus efflux from lake sediments: exploratory reactive-transport modeling. Chem Geol 236:127–147

Keighley D (2013) Outcrop chemostratigraphic correlation of the upper Green River Formation (Mahogany oil shale zone—Uinta Fm. boundary) in the Uinta Basin, Utah. Utah Geological Survey, Salt Lake City, Ut

Keighley D, Flint S (2008) Models of fluvial sandbody geometry and connectivity in the middle Green River Formation, Nine Mile Canyon, SW Uinta Basin. In: Longman MW, Morgan CD (eds) Hydrocarbon systems and production in the Uinta Basin, Utah, vol 37, Rocky Mountain Association of Geologists – Utah Geological Association, Special Publication. Rocky Mountain Association of Geologists/Utah Geological Association, Denver/Salt Lake City, pp 101–119

Keighley D, Borer J, Morgan C et al (2003a) Facies asymmetry in alluvial-lacustrine basins: a transect across the Uinta basin, eastern Utah and western Colorado. AAPG Annual Convention, Salt Lake City. 77 + xxxiii p, May 2003

Keighley D, Flint S, Howell J, Moscariello A (2003b) Sequence stratigraphy in lacustrine basins: a model for part of the Green River Formation (Eocene), southwest Uinta Basin, Utah. J Sediment Res 73:987–1006

Kleeberg A, Dudel GE (1997) Changes in extent of phosphorus release in a shallow lake (Lake Großer Müggelsee; Germany, Berlin) due to climatic factors and load. Mar Geol 139:61–75

Knudsen AC, Gunter ME (2002) Sedimentary phosphorites – an example: phosphoria formation, Southeastern Idaho, U.S.A. In: Kohn MJ, Rakovan J, Hughes JM (eds) Phosphates: geochemical, geobiological, and materials importance, vol 48, Reviews in mineralogy and geochemistry. Mineralogical Society of America, Washington, DC, pp 363–389

Lambiase JJ (1990) A model for tectonic control of lacustrine stratigraphic sequences in continental rift basins. In: Katz BJ (ed) Lacustrine basin exploration – case studies and modern analogs, vol 50, AAPG, memoir. American Association of Petroleum Geologists, Tulsa, pp 265–276

Levine SN, Stainton MP, Schindler DW (1986) A radiotracer study of phosphorus cycling in a eutrophic Canadian Shield lake, experimental lake 227, northwestern Ontario. Can J Fish Aquat Sci 43:366–378

Love D (1964) Uraniferous phosphatic lake beds of Eocene age in intermontane basins of Wyoming and Utah, U.S. Geological Survey, professional paper 474-E. U.S. Government Printing Office, Washington, DC, pp 1–66

Lowenstein TK, Demicco RV (2006) Elevated Eocene atmospheric CO_2 and its subsequent decline. Science 313:1928

Machel HG (2004) Concepts and models of dolomitization: a critical reappraisal. In: Braithwaite CJR, Rizzi G, Darke G (eds) The geometry and petrogenesis of dolomite hydrocarbon reservoirs, vol 235, Geological Society special publication. Geological Society, London, pp 7–63

Mazzullo SJ (2000) Organogenic dolomitization in peritidal to deep-sea sediments. J Sediment Res 70:10–23

Milton C, Eugster HP (1959) Mineral assemblage of the Green River Formation. In: Abelson PH (ed) Researches in geochemistry. Wiley, New York, pp 118–150

Morgan CD, Chidsey TC, McClure KP et al (2002) Reservoir characterization of the lower Green River Formation, southwest Uinta Basin, Utah. Utah Geological Survey – U.S. Department of Energy DOE/BC/15103-4 OSTI No. 805237, 140 p

Morris TH, Richmond DR (1992) A predictive model of reservoir continuity in fluvial sandstone bodies of a lacustrine deltaic system, Colton Formation, Utah. In: Fouch TD, Nuccio VF, Chidsey TC (eds) Hydrocarbon and mineral resources of the Uinta Basin, Utah and Colorado, vol 20, Utah Geological Association publication. Utah Geological Association, Salt Lake City, pp 227–236

Morrow DW (1990) Dolomite—Part 1: the chemistry of dolomitization and dolomite precipitation. Geoscience Canada, Reprint Series 4, pp 113–123

Mossman DJ, Macey JF, Lemmon PD (1987) Diagenesis in the lacustrine facies of the Albert Formation, New Brunswick, Canada: a geochemical evaluation. Bull Can Pet Geol 35:239–250

Mott LV, Drever JI (1983) Origin of uraniferous phosphatic beds in Wilkins Peak Member of Green River Formation, Wyoming. Am Assoc Pet Geol Bull 67:70–82

Mutakyahwa MKD (2002) Mineralogy and chemistry of bentonite (?) deposits at Minjingu, Lake Manyara, North Tanzania. J Afr Earth Sci 34:213–221

Nathan Y, Lucas J (1972) Synthèse de l'apatite à partir du gypse: application au problème de la formation des apatites carbonates par precipitation directe. Chem Geol 9:99–112

Picard MD (1966) Oriented, linear-shrinkage cracks in Green River Formation (Eocene), Raven Ridge area, Utah. J Sediment Petrol 36:1050–1057

Plummer PS, Gostin VA (1981) Shrinkage cracks: desiccation or synaeresis? J Sediment Petrol 51: 1147–1156

Remy R (1992) Stratigraphy of the Eocene part of the Green River Formation in the south-central part of the Uinta basin, Utah. U.S. Geological Survey, Bulletin B 1787-BB, pp BB1–BB69

Renaut RW (1993) Zeolitic diagenesis of late Quaternary fluviolacustrine sediments and associated calcrete formation in the Lake Bogoria basin, Kenya Rift Valley. Sedimentology 40:271–301

Renaut RW, Gierlowski-Kordesch EH (2010) Lakes. In: James NP, Dalrymple RW (eds) Facies models 4, vol 6, Geotext. Geological Association of Canada, St. John's, pp 541–575

Rodd JA, Stewart AD (1992) Geochemistry, weathering and diagenesis of the Diabaig Formation (Torridon Group) in NW Scotland. Scott J Geol 28:27–35

Ruttenberg KC, Berner RA (1993) Authigenic apatite formation and burial in sediments from non-upwelling, continental margin environments. Geochim Cosmochim Acta 57:991–1007

Saether OM, Runnells DD, Ristinen RA, Smythe WR (1981) Fluorine: its mineralogical residence in the oil shale of the Mahogany Zone of the Green River Formation, Piceance Creek Basin, Colorado, U.S.A. Chem Geol 31:169–184

Sakadevan K, Bavor HJ (1998) Phosphate adsorption characteristics of soils, slags, and zeolite to be used as substrates in constructed wetland systems. Water Resour 32:393–399

Slansky M (1986) Geology of sedimentary phosphates. Elsevier, New York

Smith ME, Carroll AR, Singer BS (2008) Synoptic reconstruction of a major ancient lake system: Eocene Green River Formation, western United States. Geol Soc Am Bull 120:54–84

Song Y, Hahn HH, Hoffmann E (2002) The effect of carbonate on the precipitation of calcium phosphate. Environ Technol 23:207–215

Song Y, Weidler PG, Berg U et al (2006) Calcite-seeded crystallization of calcium phosphate for phosphorus recovery. Chemosphere 63:236–243

Stamatakis MG, Koukouzas NK (2001) The occurrence of phosphate minerals in lacustrine clayey diatomite deposits, Thessaly, Central Greece. Sediment Geol 139:33–47

Strother PK, Battison L, Brasier MD, Wellman CH (2011) Earth's earliest non-marine eukaryotes. Nature 473:505–509

Stumm W, Morgan JJ (1996) Aquatic chemistry: chemical equilibria and rates in natural waters, 3rd edn. Wiley, New York

Swanson VE (1960) Oil yield and uranium content of black shales. U.S. Geological Survey, professional paper 356-A, Washington, DC, pp 1–44

Swirydczuk K, Wilkinson BH, Smith GR (1981) Synsedimentary lacustrine phosphorites from the Pliocene Glenns Ferry Formation of southwestern Idaho. J Sediment Petrol 51:1205–1214

Talbot MR, Kelts K (1986) Primary and diagenetic carbonates in the anoxic sediments of Lake Bosumtwi, Ghana. Geology 14:912–916

Taylor SR, McLennan SM (1985) The continental crust: its composition and evolution. Blackwell, London

Tuttle MLW (2009) A collection of chemical, mineralogical, and stable isotopic compositional data for Green River Oil Shale from depositional center cores in Colorado, Utah, and Wyoming. U.S. Geological Survey, Reston, Va

Tuttle MLW, Goldhaber MB (1993) Sedimentary sulfur geochemistry of the Paleogene Green River Formation, western USA: implications for interpreting depositional and diagenetic processes in saline alkaline lakes. Geochim Cosmochim Acta 57:3023–3039

United States Geological Survey (2010) USGS geochemical reference materials and certificates: USGS certificate of analysis, Green River Shale, SGR-1. http://minerals.cr.usgs.gov/geo_chem_stand/shale.html. Accessed 3 July 2010

Van Cappellen P, Berner RA (1988) A mathematical model for the early diagenesis of phosphorus and fluorine in marine sediments: apatite precipitation. Am J Sci 288:289–333

Van Cappellen P, Berner RA (1991) Fluorapatite crystal growth from modified seawater solutions. Geochim Cosmochim Acta 55:1219–1234

Vanden Berg MD, Lehle DR, Carney SM, Morgan CD (2013) Geological characterization of the Bird's Nest Aquifer, Uinta Basin, Utah: assessment of the aquifer's potential as a saline water disposal unit. Utah Geological Survey, special study 147, CD-ROM

Vozárová A, Rojkovič I (2000) Permian lacustrine phosphatic sandstone in the Southern Gemeric Unit, Western Carpathians, Slovakia. Geol Carpath 51:265–278

Wetzel RG (2001) Limnology: lake and river ecosystems, 3rd edn. Academic, San Diego